

# *FakeLocator*: Robust Localization of GAN-Based Face Manipulations via Semantic Segmentation Networks with Bells and Whistles

Yihao Huang<sup>1</sup>, Felix Juefei-Xu<sup>2</sup>, Run Wang<sup>3</sup>, Xiaofei Xie<sup>3</sup>, Lei Ma<sup>4</sup>, Jianwen Li<sup>1</sup>, Weikai Miao<sup>1</sup>,  
 Yang Liu<sup>3</sup>, Geguang Pu<sup>1</sup>,  
<sup>1</sup> East China Normal University, <sup>2</sup> Alibaba Group  
<sup>3</sup> Nanyang Technological University, <sup>4</sup> Kyushu University

## Abstract

Nowadays, full face synthesis and partial face manipulation by virtue of the generative adversarial networks (GANs) have raised wide public concern. In the digital media forensics area, detecting and ultimately locating the image forgery have become imperative. Although many methods focus on fake detection, only a few put emphasis on the localization of the fake regions. Through analyzing the imperfection in the upsampling procedures of the GAN-based methods and recasting the fake localization problem as a modified semantic segmentation one, our proposed *FakeLocator* can obtain high localization accuracy, at full resolution, on manipulated facial images. To the best of our knowledge, this is the very first attempt to solve the GAN-based fake localization problem with a semantic segmentation map. As an improvement, the real-numbered segmentation map proposed by us preserves more information of fake regions. For this new type segmentation map, we also find suitable loss functions for it. Experimental results on the CelebA and FFHQ databases with seven different SOTA GAN-based face generation methods show the effectiveness of our method. Compared with the baseline, our method performs several times better on various metrics. Moreover, the proposed method is robust against various real-world facial image degradations such as JPEG compression, low-resolution, noise, and blur.

## 1 Introduction

Everyday we receive newsletters from the media channels such as television, social media, newspaper, etc. Limited by the presentation of these media, compared with text descriptions, the information with images and videos is more trustworthy. However, within the development of digital manipulation technologies, even videos can be synthesized at a small price. In recent years, there are a lot of synthetic videos represented by celebrities [Rössler *et al.*, 2019]. Deep-Fake [deepfakes, 2017], the most famous open-source GAN-based method, has been widely used in politics and pornography. Public concerns about fraud and credibility problems

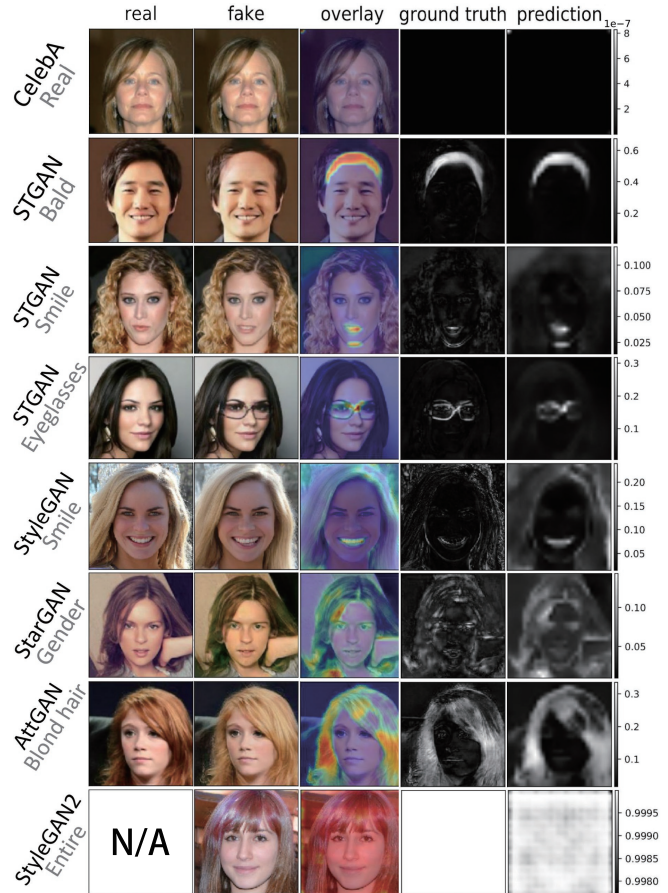


Figure 1: **Fake region localization results.** These are the results of different GANs and properties. In the left comments, CelebA is a real image database and others are GAN-based face generation methods. Gray text represents the face property. **Fake** image is produced by manipulating corresponding **real** image through GAN-based face generation method. **Ground truth** is calculated by **fake** image and **real** image. **Fake** image and **ground truth** are the input and output of our method. **Overlay** is combined of **prediction** and **fake** image. The **prediction** have colorbar which shows the value range of pixels. For the first row which uses real image of CelebA as input, for unity of the figure, we also regard it as **fake** image.

has been raised by such fake information. Hence, it is necessary to study effective and accurate methods in face forgery detection and forensics, for both reality and justice.

The images synthesized by GAN-based methods are more authentic than others. Furthermore, as a new popular technology, researchers have a great interest in detecting images generated by GAN-based methods. There are a lot of methods [Yu *et al.*, 2019; Dang *et al.*, 2018; Mo *et al.*, 2018; Wang *et al.*, 2019] proposed to classify images in a variety of ways. However, none of them considers the localization of fake regions in the fake images, which is more significant and valuable in the research field of digital image forensics.

Some forgery localization methods choose videos as the research target, mainly using **FaceForensics++** [Rössler *et al.*, 2019] database. However, many popular GAN-based methods aim at modifying other famous databases' images instead of videos. To the best of our knowledge, there are no other works focusing on the fake localization problem of these image targeting GAN-based methods except [Stehouwer *et al.*, 2019]. In the literature, they insert an attention map module into a classifier such as Xception [Chollet, 2017] to obtain the location of fake regions. The attention map module is an additional feature map added to the output of a certain convolution layer. However, the resolution of the attention map of this work is not big enough. For instance, an image of size 299x299 will obtain an attention map of size 19x19. So the attention map can not exactly pinpoint out the fake regions. In addition, the segmentation maps of all these localization methods either for videos or images have several omissions, which will be introduced and improved in our method.

To get better localization performance and higher resolution, we analyze the architecture of GAN. According to the analysis of the generator in GAN-based face generation methods, there are only three kinds of upsampling methods. The textures produced by upsampling methods contain special features, which are called **fake texture**. Regarding the fake textures as fake objects, we can use modified semantic segmentation network to locate fake objects in the images.

The main contributions are summarized as follows.

- We revisit the artifact induced by GAN-based face generation methods and use modified semantic segmentation network to locate the manipulated facial regions effectively at full resolution.
- We point out the omission in segmentation map of other localization methods and propose real-numbered segmentation map. As the problem is essentially a modified semantic segmentation problem, we find suitable loss function for it through experiments.
- Experiments are conducted on seven SOTA GAN-based face generation methods and two databases. Compared to the extant method in fake region localization of image [Stehouwer *et al.*, 2019], ours obtains a significantly better performance. Furthermore, the method is also robust against various real-world facial image degradations.

## 2 Related Work

### 2.1 GAN-based Face Manipulation

A lot of researches have put emphasis on GAN [Goodfellow *et al.*, 2014] since its emergence. IcGAN [Perarnau *et al.*, 2016] introduces the encoder that allows the network to



Figure 2: The architecture of GAN-based face generation methods

reconstruct and modify real face images with arbitrary attributes. PGGAN [Karras *et al.*, 2017] proposed progressively growing on both the generator and discriminator to obtain big high-resolution images. StarGAN [Choi *et al.*, 2018] simply uses a single model to perform image-to-image translations for multiple face properties. AttGAN [He *et al.*, 2019] applies an attribute classification constraint to the generated image to guarantee the correct change of desired attributes. STGAN [Liu *et al.*, 2019] simultaneously improves attribute manipulation accuracy as well as perception quality on the basis of AttGAN. StyleGAN [Karras *et al.*, 2019a] proposed a new generator to learn unsupervised separation of high-level attributes and stochastic variation in the generated images. Recently, StyleGAN2 [Karras *et al.*, 2019b] fixed the imperfection of StyleGAN to improve image quality.

The above GANs are the state-of-art GAN-based face generation methods. Among these GAN-based full face synthesis and partial face manipulation methods, IcGAN, AttGAN, StarGAN and STGAN are partial face manipulation methods, PGGAN and StyleGAN2 are full face synthesis methods. StyleGAN is not only a partial face manipulation method, but also a full face synthesis method. We verify the effectiveness of our method on these seven GAN-based methods. In the following content, every mention of **seven GAN-based face generation methods** is referred to the GANs introduced here.

### 2.2 Manipulated Face Localization

Several works have been proposed on the manipulated face localization problem. [Songsri-in and Zafeiriou, 2019] proposes an architecture to predict face forensic localization. [Nguyen *et al.*, 2019] uses multi-task learning approach to simultaneously detect manipulated videos and locate the manipulated regions. [Li *et al.*, 2019] proposes face X-ray to locate the fake regions with smaller training dataset than other methods. They all use CNN-based methods to locate the manipulated region in videos.

[Stehouwer *et al.*, 2019] presents the first and only technique that applies the attention mechanism to address the problem on images. The attention map is advantageous to be added into arbitrary networks and help to improve detection accuracy. However, the attention map is too small to point out the specific fake regions. Furthermore, the segmentation maps used by these methods are all incomplete, which lose information of fake regions.

### 2.3 Semantic Segmentation Network

In classical image tasks, the semantic segmentation task is defined to identify the object category of each pixel for every known object within an image. The label of each pixel is class-aware. For example, in a view of street, a semantic segmentation network can label whether a pixel belongs to people or cars. This is very useful in pilotless automobile.

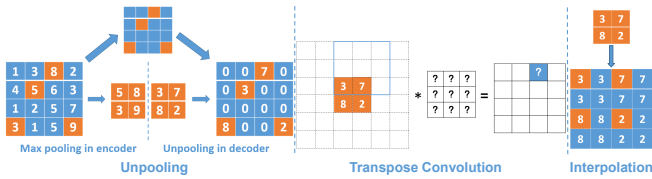


Figure 3: Upsampling methods

FCN [Long *et al.*, 2015] introduces the basic idea to apply deep learning to the semantic segmentation task.

### 3 Imperfection of GAN-based methods

#### 3.1 Architecture

There are mainly two ways to generate face images: full face synthesis and partial face manipulation. We call these two methods **face generation methods**. Their architecture can be summarized as an encoder-decoder framework.

As shown in Figure 2, for all the partial face manipulation methods, the encoder compresses the real image into some small feature maps by convolution and pooling layers. Changing the feature maps with specific face properties, the modified feature maps are amplified by the upsampling layers in the decoder to be a high-resolution fake image. In full face synthesis, the input is a random vector. Similarly, it also needs to go through a decoder to become an entire fake face image. We can find that all the GAN-based face generation methods have the procedure which amplifies the images from low-resolution to high-resolution. In magnification process, images are inserted with a lot of new pixels calculated by existing pixels. Hence, the output fake face images of these GAN-based methods inevitably contain fake texture which can not be obtained from the real world through a camera.

#### 3.2 Upsampling

Upsampling is a technique that can improve the image resolution. There are three kinds of upsampling methods: unpooling, transpose convolution and interpolation. Figure 3 demonstrates the specific way of these methods. For GAN-based methods, the most commonly used interpolations are nearest neighbor interpolation, bilinear interpolation and bicubic interpolation. Here in Figure 3 we just show nearest neighbor interpolation as an example.

After analyzing the code of seven GAN-based face generation methods, we find that only transpose convolution and interpolation have been used. IcGAN uses interpolation and others use transpose convolution.

Although only two methods are used, all of these three methods have been proved inducing fake texture. Google Brain [Odena *et al.*, 2016] has proved that the transpose convolution will result in the checkerboard texture of the output image. [Zhang *et al.*, 2019] has proved that the transpose convolution and nearest neighbor interpolation have fake texture. Though not mentioned explicitly, the process of their proof also points out that unpooling will produce fake texture. For the remaining bilinear and bicubic interpolations, they will bring periodicity into the second derivative signal of images [Gallagher, 2005]. This means that the interpolated images exist fake texture which can be detected by convolution kernel, for instance, Laplace operator.

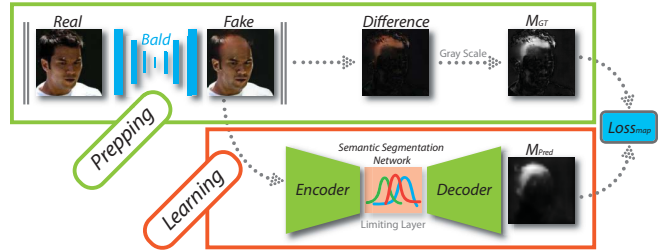


Figure 4: Framework of our methodology

## 4 Proposed Method

If we treat the regions of fake texture as fake objects and regions of real texture as real objects, the fake region localization problem can be regarded as a task of finding the fake objects in the image. As for the latter, the method based on semantic segmentation network can solve it effectively.

However, this is not a traditional semantic segmentation problem. For the sake of distinction, we call the segmentation map proposed by us **real-numbered segmentation map** while that in traditional semantic segmentation problem is **integer segmentation map**. The real-numbered segmentation map preserves more information of fake regions and is totally different from integer segmentation map. The pixel values in integer segmentation map are all integers. While in real-numbered segmentation map, the pixel values are real numbers in range  $[0,1]$ . Through experiments, we choose a suitable loss function to make real-numbered segmentation map effective. In this section, we will also introduce the data preprocessing method and the framework of our method.

One advantage of the approach is, as long as the upsampling methods produce special features, the method is effective. Because the method is designed for the imperfection of the upsampling methods and it is almost inevitable for GAN-based face generation methods to use upsampling methods. Furthermore, withing the development of semantic segmentation networks, our method will achieve a better performance on fake localization problem.

### 4.1 Framework

Figure 4 shows the framework of our methodology. The backbone network is undoubtedly a semantic segmentation network. The input is a fake image ( $X'$ ) while the output is a prediction segmentation map ( $M_{Pred}$ ).  $M_{Pred} = \mathcal{G}_{dec}(\mathcal{G}_{enc}(X') \mapsto [0, 1])$ , where  $\mathcal{G}_{dec}$  and  $\mathcal{G}_{enc}$  are the decoder and encoder of the semantic segmentation network.  $M_{GT}$  represents the ground truth segmentation map. Semantic segmentation network is an encoder-decoder architecture. It should be noted that usually the network is designed to predict many categories and the pixels of output segmentation map are integers. In our method, the pixel values in the segmentation map are real numbers. So we should fine-tune the network and limit the pixel values in the prediction segmentation map. We add a limiting layer between the encoder and the decoder so that the pixel values could be limited to range within  $[0,1]$ . This limiting layer can also be added after the decoder. The loss ( $\mathcal{L}_{map}$ ) is simply calculated by the following formula. Here  $\mathcal{L}$  will be introduced in subsection 4.3.

$$\mathcal{L}_{map} = \mathcal{L}(M_{Pred}, M_{GT}) \quad (1)$$

Furthermore, we add a classifier to the semantic segmentation network. It is just added for facilitating the calculation of the accuracy on detecting whether an image is real or fake. The classifier is not necessary for that we can judge the authenticity of the input image through the segmentation map. In the experiment, we has verified that the network with or without classifier has similar performance and they are both effective in locating fake regions.

## 4.2 Data Pre-process

The training samples consist of two parts: input image and segmentation map. The input images fall into two categories, real images and fake images. For a training sample which regards the real image as the input image, the corresponding segmentation map is a gray-scale map with all the pixel values equal to 0. This means in the current input image, there is no fake texture, in other words, no fake object. On the other hand, if the input image is a fake image, the segmentation map is obtained by the following calculating procedure.

As shown in Figure 5, these images in turn are real image ( $\mathbf{X}$ ), fake image ( $\mathbf{X}'$ ), real-numbered segmentation map ( $\mathbf{M}$ ) and binary segmentation map ( $\mathbf{B}$ ).  $\mathbf{X}, \mathbf{X}' \in \mathbb{R}^{H \times W \times 3}$  and  $\mathbf{M}, \mathbf{B} \in \mathbb{R}^{H \times W \times 1}$ , where  $H, W$  are height and width of these images. The fake image is produced by adding property  $p$  to the real image.  $\mathbf{X}' = \mathcal{G}_{dec,F}(\mathcal{G}_{enc,F}(\mathbf{X}), p)$ , where  $\mathcal{G}_{dec,F}$  and  $\mathcal{G}_{enc,F}$  are the decoder and encoder of the method  $F$ ,  $F \in \{\text{all the partial face manipulation GANs}\}$ . To achieve the real-numbered segmentation map, there are three steps as follows. 1) calculate the pixel difference between the real image and the fake image. 2) take the absolute value of the result and turn it into a gray-scale map. 3) divide each pixel by 255. Then each pixel value locates in the range of  $[0,1]$ . Equation (2) shows the the formula, in which  $\mathbf{X}_{i,j,k}, \mathbf{X}'_{i,j,k}$  ( $1 \leq i \leq H, 1 \leq j \leq W, 1 \leq k \leq 3, 0 \leq \mathbf{X}_{i,j,k}, \mathbf{X}'_{i,j,k} \leq 255$ ) are the value of a channel of a pixel of  $\mathbf{X}$  and  $\mathbf{X}'$  respectively.  $\mathbf{M}_{i,j}, \mathbf{B}_{i,j}$  ( $1 \leq i \leq H, 1 \leq j \leq W, 0 \leq \mathbf{M}_{i,j} \leq 1, \mathbf{B}_{i,j} \in \{0, 1\}$ ) are the value of a pixel of  $\mathbf{M}$  and  $\mathbf{B}$  respectively. Gray is a function converts RGB pixel to gray-scale pixel.

$$\mathbf{M}_{i,j} = \text{Gray}(|\mathbf{X}_{i,j,k} - \mathbf{X}'_{i,j,k}|)/255 \quad (2)$$

For the full face synthesis, the segmentation map is a gray-scale map with all the pixel values equal to 1. The real-numbered segmentation map clearly depicts the difference between the real and fake images and highlights the regions with large differences.

We are primarily concerned with the property modified by the GAN-based method. Thus when modifying a face property, the mainly modified regions caused by that property should be distinguished from the rest regions which are incidentally caused by the imperfection of GAN-based method. Here pixels with higher value, which represent light regions, are the fake regions that we care about. So in the prediction segmentation map, the light regions also represent the modified regions where we are mainly interested in. In other words, the light regions are fake regions.

Other image forgery localization methods use the segmentation maps as **binary segmentation maps**, which are essentially a subset of integer segmentation maps with the pixel



Figure 5: From left to right: real image, fake image, real-numbered segmentation map and binary segmentation map

values either 0 or 1. They usually use thresholds to produce binary segmentation maps. The pixel values bigger than the threshold become 1 while the others become 0. This binary segmentation map has several omissions. Firstly, it omits all the information of fake regions less than the threshold. Secondly, the threshold is usually a fixed value defined by experience, which does not work in all cases. Finally, the values of manipulated pixels in the fake image are all less than threshold if the fake image is minorly manipulated. The corresponding binary segmentation map thus turns out to be entire black and far from the truth.

## 4.3 Loss Function

For the real-numbered segmentation map, we applied four commonly used losses in traditional semantic segmentation problems. In the experiment, we find that L1 loss and L2 loss are the better choices than the others. Their formulas are shown in Equation (3).  $\mathbf{X}_{i,j}$  and  $\mathbf{Y}_{i,j}$  ( $1 \leq i \leq H, 1 \leq j \leq W$ ) represent the pixel in the prediction real-numbered segmentation map and ground truth of the real-numbered segmentation map respectively, where  $H, W$  are the height and width of the maps.

$$\mathcal{L}1_{loss} = \frac{1}{n} \sum |\mathbf{X}_{i,j} - \mathbf{Y}_{i,j}| \quad \mathcal{L}2_{loss} = \frac{1}{n} \sum |\mathbf{X}_{i,j} - \mathbf{Y}_{i,j}|^2 \quad (3)$$

## 5 Experimental Result

### 5.1 Experimental Setup

**Databases:** Our experiment benchmarks the real face databases CelebFaces Attributes (CelebA) [Liu *et al.*, 2015] and Flickr-Faces-HQ (FFHQ) [Karras *et al.*, 2019a]. CelebA contains 202,599 face images of celebrities, each annotated with 40 binary attributes. FFHQ contains 70,000 high-quality images. The database includes vastly more variation than CelebA in terms of age, ethnicity and image background.

The real images are from CelebA and FFHQ databases. The fake images are produced by seven GAN-based face generation methods and their corresponding databases and properties, as shown in Table 1. The images are all in PNG format. We use **Entire** to represent the property of the images produced by full face synthesis methods.

**Settings:** The experiment runs on a Ubuntu 16.04 system with an Intel(R) Xeon(R) CPU E5-2699 with 196 GB of RAM. The server also has a NVIDIA RTX 2080ti GPU with 11G of RAM. In the experiment, we train for 10 iterations with an ADAM [Kingma and Ba, 2014] optimizer whose  $\alpha = 0.0001, \beta_1 = 0.99, \beta_2 = 0.999$ , and weight decay =  $10^{-7}$ . The minibatch size of every training and validation dataset is 8.

**Training and Test Dataset:** In the seven GAN-based face generation methods, STGAN is the newest GAN-based

Table 1: Properties of GANs

STGAN (CelebA)	AttGAN (CelebA)
Bald, Bangs, Black hair, Blond hair, Smile, Brown hair, Eyeglasses, Male, Mustache	Bald, Bangs, Black hair, Blond hair, Brown hair, Eyeglasses, Male, Smile
StarGAN (CelebA)	IcGAN (CelebA)
Black hair, Blond hair, Brown hair, Gender, Age	Bald, Bangs, Eyeglasses, Smile
StyleGAN (FFHQ)	PGGAN (FFHQ), StyleGAN (FFHQ), StyleGAN2 (FFHQ)
Smile, Age, Gender	Entire

method in partial face manipulation and achieves the state-of-art results. Thus we choose it as the main experiment object to demonstrate our method. Of course, we also confirm the availability of our method on other GANs, which is also shown in Figure 1 and Table 4.

For each face property, we train the model with 5000 persons’ real images and fake images of other different 5000 persons. In the test dataset, we use 1000 real images and 1000 fake images to calculate classification metric. For segmentation metric, we reuse the 1000 fake images. The images in the test and training dataset are based on different persons.

**Network:** We utilize the Deeplabv3 architecture as our backbone network. Deeplabv3 has a good performance and Pytorch [Paszke *et al.*, 2019] provides a pre-trained Deeplabv3-ResNet101 model. Deeplabv3-ResNet101 is constructed by a Deeplabv3 model with a ResNet-101 backbone. The pre-trained model has been trained on a subset of COCO train2017, on the 20 categories that are present in the Pascal VOC dataset. We fine-tune the network and use **Sigmoid** function as the limiting layer. The input size supported by Deeplabv3-ResNet101 is 224x224, thus we resized all the input images to this size. Other semantic segmentation network are also available. We just need to adjust the input image to the corresponding size according to their architecture.

**Metrics:** We report ACC (Accuracy) for classification and use COSS (Cosine Similarity), PSNR (Peak Signal-to-noise Ratio) and SSIM (Structural Similarity) for segmentation. Cosine similarity is a measure of similarity between two non-zero vectors of an inner product space that measures the cosine of the angle between them. We transform the image to vector before calculating COSS. PSNR is the most commonly used measurement for the reconstruction quality of lossy compression. SSIM is used for measuring the similarity between two images. ACC, COSS, PSNR and SSIM metrics are better if a higher value is provided. The value range of ACC, COSS and SSIM are all in [0,1].

## 5.2 Results and Analysis

To evaluate the effectiveness of our new approach, experiments try to cover the following four research questions:

**RQ1: As the output is real-numbered segmentation map, which loss function is suitable for fake region localization problem?** In Table 2, we show a comparison of the results with different loss function strategies. Here we choose *Bald* of STGAN as the property of fake images. In the first column, **Baseline** represents the result of [Stehouwer *et al.*, 2019]. We enlarge its prediction segmentation maps to the

Table 2: Loss Function Comparison

	ACC	COSS	PSNR	SSIM
<b>Baseline [Stehouwer’19]</b>	1.0	0.5008	5.17	0.1591
L1 Loss ( <i>no cl</i> )	\	<b>0.9271</b>	22.54	0.7533
L1 Loss	0.994	0.8887	22.83	<b>0.7823</b>
L2 Loss	1.0	0.9228	<b>23.09</b>	0.7497
Dice Loss	0.990	0.7633	12.89	0.3585
Focal Loss	0.984	0.3988	20.79	0.3301

Table 3: Universal Test

	STGAN	AttGAN			STGAN	StyleGAN		
	Bald	Bald	Black hair	Eyeglasses	Smile	Smile	Age	Gender
DR	0.994	0.973	0.513	0.519	1.0	0.588	0.593	0.588
PSNR	22.83	21.46	22.84	23.52	35.49	20.85	18.59	16.50
SSIM	0.7823	0.6688	0.3966	0.4168	0.9218	0.5571	0.4958	0.4301
Cosine	0.8887	0.8141	0.6932	0.6950	0.8844	0.6176	0.3141	0.6470

size of 224x224 before calculating the metrics. The label *no cl* means the model does not have a classifier.

Compared to **Baseline**, the segmentation maps predicted by our method not only have a higher resolution, but also a better performance. Furthermore, using the same loss function strategy, Deeplabv3 with/without classifier achieves a similar value on metrics. Thus the classifier used to calculate ACC does not affect the prediction segmentation map. The highest value of PSNR and SSIM are achieved by L1 loss and L2 loss respectively. Their performances are approximate and better than other loss functions. We can conclude that the loss functions outstanding in regression problems are better for real-numbered segmentation map. In the following experiments, considering the sake of unity, we choose L1 loss as the default loss function.

**RQ2: What is the performance of our method across different GANs?** In the experiment, we find that our method is efficient for all the GANs and their specified face properties. Hence there is a further question. Is the model trained on one GAN is effective for other GANs?

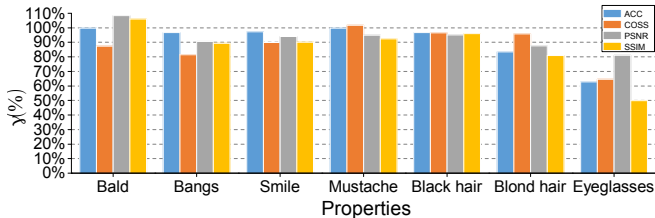
As shown in Table 3, we demonstrate some of the test results. Here are two different test pairs. The model trained from STGAN (Bald) tests properties of AttGAN and the model trained from STGAN (Smile) tests properties of StyleGAN. The gray columns are the first column of each test pair. It records the value of the model testing on the test dataset of itself, which is used as the reference substance. For each test pair, the three columns right beside the gray column are the performance of the model on other datasets.

We can find that the model trained by one GAN and specified property will be more effective on other GANs with the same dataset and property than the GANs with different datasets or properties. Furthermore, in our observation from a large number of experiments, the model trained by one GAN and specified property also does not have a good performance on the same GAN with other properties. To solve this problem, we introduce the method in the next question.

**RQ3: How to improve the universality of the method?** We train a model with many single-face-property fake images. We select STGAN, StyleGAN, AttGAN, StarGAN, IcGAN, PGGAN, StyleGAN2 and all their properties. Each category  $C_{i,j}$  ( $i \in \text{GANs}$ ,  $j \in \text{Properties of GANs}(i)$ ) supports

Table 4: Performance of The Model

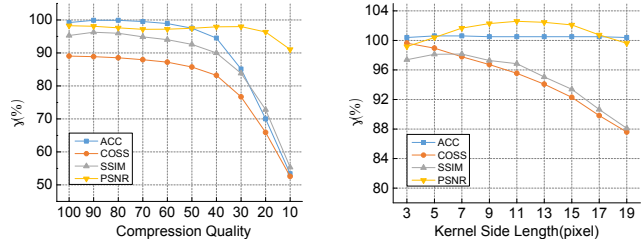
	STGAN						StyleGAN				StarGAN			AttGAN			IcGAN	PGGAN	StyleGAN2
	Smile	Bangs	Bald	Mustache	Eyeglasses	Black hair	Age	Gender	Smile	Entire	Age	Gender	Black hair	Bald	Smile	Eyeglasses	Bald	Entire	Entire
ACC	0.9985	0.9985	<b>0.9985</b>	0.9935	0.997	0.9985	0.9985	0.999	0.999	0.921	0.999	0.999	0.999	0.9985	0.9985	0.9985	0.9995	0.9775	0.855
PSNR	34.72	33.07	<b>27.51</b>	36.59	33.23	31.05	20.71	18.92	22.68	55.08	26.38	26.71	25.25	25.31	29.49	28.19	17.57	48.70	72.00
SSIM	0.9086	0.9033	<b>0.8572</b>	0.8829	0.8663	0.9029	0.6159	0.5726	0.6625	0.8268	0.7929	0.7952	0.7911	0.7839	0.8736	0.8207	0.6002	0.8945	0.9262
COSS	0.8634	0.8850	<b>0.9014</b>	0.9152	0.9093	0.8817	0.7479	0.7580	0.7365	0.9174	0.8494	0.8416	0.8780	0.8883	0.8277	0.8313	0.8352	0.9972	0.9678

Figure 6: Comparison with no disorganization.  $\gamma$  means the percentage of the metric values compared with no disorganization.Figure 7: Disorganization test result. This is the property *Blond hair* of STGAN.

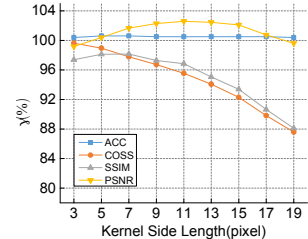
2000 fake images into the training dataset. There are totally 64000 fake images and 64000 real images randomly selected in CelebA and FFHQ. The model performs well on the test dataset, which is shown in Table 4. The real-numbered segmentation maps corresponding to these index values are referred to Figure 1. In addition, even though the model uses a lot of GANs and properties for training, in the test dataset, it only labels the location of fake regions of the changed face properties. This is a nice phenomenon which demonstrates that the model has learned to recognize the fake textures and distinguish them. This method not only improves the universality, but also improves the performance. The metric value of STGAN (Bald) is significantly higher than that in Table 2.

**RQ4: How robust is the model?** To test the robustness of the model, we use two different test directions. First, we crop each fake image uniformly into four pieces and splice them randomly, which is called the *disorganization test*. The purpose of this test is to verify whether the model is strongly correlated to the location, namely it just remembers the location instead of recognizing the fake texture. Figure 6 demonstrates the percentage of the metric values compared to that before disorganization test. The model performance is just a little worse than formal situation. Figure 7 shows the prediction result of the disorganization test.

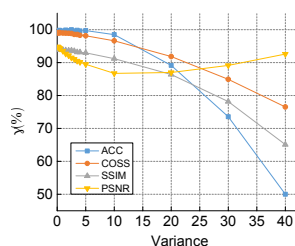
We also apply four different real-world facial image degradations (**JPEG Compression**, **Blur**, **Noise**, **Low-resolution**) on 1000 fake images. The real-numbered segmentation map is processed by the real image and degradation fake image. In Figure 8, the vertical axes of all the four subfigures represent the percentage of the metric values compared to that before degradation. **JPEG Compression** means converting image from PNG format to JPEG format. The horizontal axis of the image represents the compression quality during conversion.



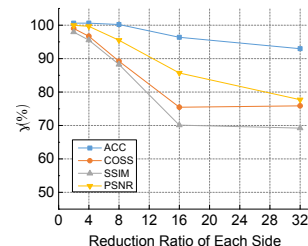
(a) JPEG Compression



(b) Blur



(c) Noise



(d) Low-resolution

Figure 8: Anti-degradation capability Of the model.  $\gamma$  means the percentage of the metric values compared with no degradation.

**Blur** and **Noise** mean applying Gaussian blur and Gaussian noise to fake images respectively. The horizontal axis respectively represents the filter size of the Gaussian blur and the variance of the Gaussian noise. **Low-resolution** means resizing the fake image to a low resolution, then restoring to original resolution. The quality of the fake image will reduce in resizing procedure. The horizontal axis represents the reduction ratio of each side of the image.

We can find that all the metric values gradually reduce in **Low-resolution**. In the other three degradations, **PSNR** achieves only minor changes, while **ACC**, **COSS** and **SSIM** decrease when the interference is extremely high. Overall, our methodology performs well against various degradations.

## 6 Conclusion

In this paper, we utilize the imperfection of the upsampling procedure in all the GAN-based partial face manipulation methods and full face synthesis methods. Regarding the fake textures as fake objects, we recast the fake localization problem as a modified semantic segmentation one. Through using modified semantic segmentation networks with bells and whistles, we achieve the SOTA localization accuracy.

In future work, we think there are two ways deserve researching. One is to propose new upsampling methods which do not contain special rules. That will make the images generated by GAN-based methods more realistic. The other is to visualize the fake texture in each image and classify them according to different GANs and upsampling methods.

## References

- [Choi *et al.*, 2018] Yunjey Choi, Minje Choi, Munyoung Kim, Jung-Woo Ha, Sunghun Kim, and Jaegul Choo. StarGAN: Unified generative adversarial networks for multi-domain image-to-image translation. In *Proceedings of the IEEE Conference on Computer Vision and Pattern Recognition*, pages 8789–8797, 2018.
- [Chollet, 2017] François Chollet. Xception: Deep learning with depthwise separable convolutions. In *Proceedings of the IEEE conference on computer vision and pattern recognition*, pages 1251–1258, 2017.
- [Dang *et al.*, 2018] L Dang, Syed Hassan, Suhyeon Im, Jaechol Lee, Sujin Lee, and Hyeonjoon Moon. Deep learning based computer generated face identification using convolutional neural network. *Applied Sciences*, 8(12):2610, 2018.
- [deepfakes, 2017] deepfakes. faceswap. <https://github.com/deepfakes/faceswap>, 2017.
- [Gallagher, 2005] Andrew C Gallagher. Detection of linear and cubic interpolation in jpeg compressed images. In *CRV*, volume 5, pages 65–72. Citeseer, 2005.
- [Goodfellow *et al.*, 2014] Ian Goodfellow, Jean Pouget-Abadie, Mehdi Mirza, Bing Xu, David Warde-Farley, Sherjil Ozair, Aaron Courville, and Yoshua Bengio. Generative adversarial nets. In *Advances in neural information processing systems*, pages 2672–2680, 2014.
- [He *et al.*, 2019] Zhenliang He, Wangmeng Zuo, Meina Kan, Shiguang Shan, and Xilin Chen. AttGAN: Facial attribute editing by only changing what you want. *IEEE Transactions on Image Processing*, 2019.
- [Karras *et al.*, 2017] Tero Karras, Timo Aila, Samuli Laine, and Jaakko Lehtinen. Progressive growing of GANs for improved quality, stability, and variation. *arXiv preprint arXiv:1710.10196*, 2017.
- [Karras *et al.*, 2019a] Tero Karras, Samuli Laine, and Timo Aila. A style-based generator architecture for generative adversarial networks. In *Proceedings of the IEEE Conference on Computer Vision and Pattern Recognition*, pages 4401–4410, 2019.
- [Karras *et al.*, 2019b] Tero Karras, Samuli Laine, Miika Aittala, Janne Hellsten, Jaakko Lehtinen, and Timo Aila. Analyzing and improving the image quality of styleGAN. *arXiv preprint arXiv:1912.04958*, 2019.
- [Kingma and Ba, 2014] Diederik P Kingma and Jimmy Ba. Adam: A method for stochastic optimization. *arXiv preprint arXiv:1412.6980*, 2014.
- [Li *et al.*, 2019] Lingzhi Li, Jianmin Bao, Ting Zhang, Hao Yang, Dong Chen, Fang Wen, and Baining Guo. Face x-ray for more general face forgery detection. *arXiv preprint arXiv:1912.13458*, 2019.
- [Liu *et al.*, 2015] Ziwei Liu, Ping Luo, Xiaogang Wang, and Xiaoou Tang. Deep learning face attributes in the wild. In *Proceedings of the IEEE international conference on computer vision*, pages 3730–3738, 2015.
- [Liu *et al.*, 2019] Ming Liu, Yukang Ding, Min Xia, Xiao Liu, Errui Ding, Wangmeng Zuo, and Shilei Wen. StGAN: A unified selective transfer network for arbitrary image attribute editing. In *Proceedings of the IEEE Conference on Computer Vision and Pattern Recognition*, pages 3673–3682, 2019.
- [Long *et al.*, 2015] Jonathan Long, Evan Shelhamer, and Trevor Darrell. Fully convolutional networks for semantic segmentation. In *Proceedings of the IEEE conference on computer vision and pattern recognition*, pages 3431–3440, 2015.
- [Mo *et al.*, 2018] Huaxiao Mo, Bolin Chen, and Weiqi Luo. Fake faces identification via convolutional neural network. In *Proceedings of the 6th ACM Workshop on Information Hiding and Multimedia Security*, pages 43–47. ACM, 2018.
- [Nguyen *et al.*, 2019] Huy H Nguyen, Fuming Fang, Junichi Yamagishi, and Isao Echizen. Multi-task learning for detecting and segmenting manipulated facial images and videos. *arXiv preprint arXiv:1906.06876*, 2019.
- [Odena *et al.*, 2016] Augustus Odena, Vincent Dumoulin, and Chris Olah. Deconvolution and checkerboard artifacts. *Distill*, 2016.
- [Paszke *et al.*, 2019] Adam Paszke, Sam Gross, Francisco Massa, Adam Lerer, et al. PyTorch: An imperative style, high-performance deep learning library. In *Advances in Neural Information Processing Systems*, pages 8024–8035, 2019.
- [Perarnau *et al.*, 2016] Guim Perarnau, Joost van de Weijer, Bogdan Raducanu, and Jose M. Álvarez. Invertible Conditional GANs for image editing. In *NIPS Workshop on Adversarial Training*, 2016.
- [Rössler *et al.*, 2019] Andreas Rössler, Davide Cozzolino, Luisa Verdoliva, Christian Riess, et al. FaceForensics++: Learning to detect manipulated facial images. *arXiv preprint arXiv:1901.08971*, 2019.
- [Songsri-in and Zafeiriou, 2019] Kritaphat Songsri-in and Stefanos Zafeiriou. Complement face forensic detection and localization with facial landmarks. *arXiv preprint arXiv:1910.05455*, 2019.
- [Stehouwer *et al.*, 2019] Joel Stehouwer, Hao Dang, Feng Liu, Xiaoming Liu, and Anil Jain. On the detection of digital face manipulation. *arXiv preprint arXiv:1910.01717*, 2019.
- [Wang *et al.*, 2019] Run Wang, Lei Ma, Felix Juefei-Xu, Xiaofei Xie, Jian Wang, and Yang Liu. Fakespotter: A simple baseline for spotting AI-synthesized fake faces. *arXiv preprint arXiv:1909.06122*, 2019.
- [Yu *et al.*, 2019] Ning Yu, Larry S Davis, and Mario Fritz. Attributing fake images to GANs: Learning and analyzing GAN fingerprints. In *Proceedings of the IEEE International Conference on Computer Vision*, pages 7556–7566, 2019.
- [Zhang *et al.*, 2019] Xu Zhang, Svebor Karaman, and Shih-Fu Chang. Detecting and simulating artifacts in GAN fake images. *arXiv preprint arXiv:1907.06515*, 2019.